Baku State University: Journal of Physics & Space Sciences, **2025**, v2 (3), p. 63-77

journal homepage: http://bsuj.bsu.edu.az/en

Structural and Optical Behavior of Commercial vs. Synthesized ZnO Nanoparticles Doped with Europium via Wet Impregnation

Sevinj G. Nuriyeva[*1], Aynura H. Karimova[3], Flora V. Hajiyeva[2]

[1]Nano Research Laboratory, Center of Excellence in Research,
Development and Innovation, Baku State University, Baku, Azerbaijan.
[2]Department of Chemical Physics of the Nanomaterials, Baku State University, Baku, Azerbaijan,
[3]Department Chemistry of High Molecular Weight Compounds, Baku AZ 1148, Azerbaijan,
Received 01-Jul-2025; Accepted 14-Aug-2025
DOI: https://doi.org/10.30546/209501.101.2025.2.03.032

Abstract

Zinc oxide (ZnO) nanoparticles are promising functional nanomaterials with tunable electronic and optical properties, which can be further enhanced through rare-earth doping. In this work, the structural and optical behavior of europium-doped ZnO nanoparticles obtained from two different sources–commercially available ZnO (C) and ZnO (S) synthesized via co-precipitation–is investigated. ZnO nanoparticle types were subjected to europium incorporation by a wet impregnation approach. Comprehensive structural and optical characterization, including X-ray diffraction (XRD), scanning electron microscopy (SEM), transmission electron microscopy (TEM), UV–Vis absorption, and photoluminescence (PL), was carried out to evaluate the influence of europium on crystal structure, morphology, and optical response. The comparison revealed distinct differences between the commercial and synthesized systems in terms of particle morphology, crystallinity, band gap, and emission behavior, providing new insights into how precursor source affects the doping outcome and functional performance of europium modified ZnO.

Keywords: Commercial ZnO NPs, synthesized ZnO NPs; Europium doping (Eu^{3+}); Wet impregnation.
PACS Numbers: 81.07.-b

[*]*Corresponding author* – Tel.: (+994) 50 257 71 87
e-mail: snuriyeva@bsu.edu.az; *ORCID ID*: 0000-0003-0331-6556

1. Introduction

Among various luminescent materials, wide-bandgap semiconductor oxides have recently attracted considerable research attention due to their exceptional optical properties and multifunctionality. Zinc oxide (ZnO), an II–VI group semiconductor, is particularly notable for its wide and direct bandgap (~3.37 eV at room temperature), making it highly responsive to ultraviolet (UV) radiation. Furthermore, its high exciton binding energy (~60 meV) enables efficient excitonic recombination even at ambient conditions, positioning ZnO as an excellent material for UV light emission [1-3]. These characteristics make ZnO nanostructures–such as nanoparticles, nanorods, and nanowires–promising candidates for a wide range of applications in optoelectronics and photonics, including UV light-emitting diodes (LEDs), laser diodes, gas sensors, transparent conducting films, photodetectors, and solar cells.

ZnO nanoparticles (NPs) with various morphologies can be synthesized via numerous physical and chemical techniques, such as chemical vapor deposition, metal-organic chemical vapor deposition, thermal evaporation, sol-gel methods, hydrothermal synthesis, molecular beam epitaxy, and solvothermal growth [4].

The optical behavior of ZnO nanostructures is primarily governed by their photoluminescence (PL), which typically shows two main emission regions: near-band-edge (NBE) UV emission and broad visible emission. NBE emission arises from free exciton recombination close to the bandgap energy, while the visible emission originates mainly from intrinsic defect states. These emissions are highly sensitive to the synthesis conditions, morphology, and crystallinity. ZnO's broad visible luminescence, covering the 1.65–3.1 eV range, results from deep-level defects and includes blue, green, and yellow components. Blue emission is often associated with zinc vacancies or oxygen antisites, while green emission (~2.4–2.5 eV) typically results from oxygen vacancies, interstitial zinc, or transitions involving shallow donor levels [5]. The prevalence and nature of these defects depend strongly on the synthesis parameters, particularly whether the environment is zinc-rich or oxygen-deficient.

Due to its excellent luminescence efficiency and broad defect-related emissions in the visible spectrum, ZnO is widely used in optical sensing, lighting, and bioimaging. Its low toxicity and high biocompatibility make it especially suitable as a fluorescent marker in biomedical diagnostics. Moreover, ZnO-based PL has been effectively utilized for detecting gases, humidity, and other environmental parameters, demonstrating its potential for advanced sensing technologies [6].

Despite these advantages, pure ZnO exhibits relatively weak and unstable emission in the visible region. While it displays strong UV NBE emission due to intrinsic defects–mainly oxygen vacancies and zinc interstitials–its visible luminescence is generally broad, weak, and difficult to control, which limits its applicability in sys-

tems requiring consistent and tunable visible emission. To overcome these limitations and enhance ZnO's luminescent performance, various doping strategies have been explored [7-9]. Among them, rare-earth ion doping has emerged as an effective method for improving both emission intensity and spectral tunability.

In addition to modifying the optical behavior, doping significantly alters the structural properties of ZnO, including crystallinity, particle size, and defect density, which in turn affect its electrical, optical, and mechanical performance. Depending on the type of dopant and its incorporation mechanism, ZnO can function as a luminescent material or as a phosphor, especially when doped with rare-earth or transition metal ions [10-11].

Rare-earth ions are known for their sharp and characteristic emissions in the visible and infrared regions, making them highly suitable for various photonic applications. For example, Eu^{3+} ions provide intense red emission ($^5D_0 \rightarrow {}^7F_2$), making them ideal for applications in white LEDs, displays, and sensors. Tb^{3+} and Er^{3+} ions emit green and infrared light, respectively, and are widely used in LED and fiber-optic technologies. Eu^{3+}-doped ZnO nanomaterials have shown great promise in red phosphors, optical sensors, white LEDs, and bioimaging due to their enhanced emission efficiency and extended spectral range [12-13].

The effectiveness of Eu^{3+} doping in ZnO largely depends on the synthesis method, which determines how the ions are incorporated into the lattice–either by substituting Zn^{2+} or occupying interstitial sites. These incorporation mechanisms directly affect defect formation, dopant distribution, and ultimately, PL behavior. Techniques such as hydrothermal synthesis, sol-gel processing, and solid-state reactions differ in their ability to control these parameters. Therefore, the choice of synthesis route and dopant concentration is critical for tailoring the structural and optical properties of ZnO for specific applications in photonics, sensors, and energy devices [14-15].

Doping ZnO NPs with Eu^{3+} ions enhance their luminescent properties, mainly through the sharp red emission (~615 nm) corresponding to the $^5D_0 \rightarrow {}^7F_2$ transition of Eu^{3+}. These ions serve as luminescent centers within the ZnO matrix, enabling efficient energy transfer and improving both emission intensity and stability. Moreover, the inclusion of Eu^{3+} can induce local lattice distortions and alter defect states, which further modulate the optical properties.

Despite the extensive research on Eu^{3+}-doped ZnO for enhanced luminescence, many studies are limited using a single synthesis method without systematic comparisons under well-controlled conditions. The effects of different doping techniques–particularly in-situ versus post-synthesis methods–on structural integrity, defect distribution, and optical performance are not yet fully understood.

This study aims to investigate the influence of Eu^{3+} doping introduced by the wet impregnation method on two types of ZnO nanoparticles: commercially available and laboratory synthesized. The work focuses on how the origin of ZnO nanopartic-

les affects lattice distortion, crystallite size, bandgap energy, and photoluminescence properties, with particular attention to Eu-related red emission. By correlating the structural modifications with optical behavior, the study provides insights into the structure–property relationships of Eu-doped ZnO nanomaterials, contributing to the rational design of high-performance materials for optoelectronic and photonic applications.

2. Experimental

2.1. Materials

The precursors used for the synthesis of ZnO nanoparticles (NPs) included zinc acetate dihydrate (Zn $(CH_3COO)_2 \cdot 2H_2O$, 99.0%) and sodium hydroxide (NaOH, 99.9%). Europium (Eu^{3+}) ion doping was performed using europium metal powder (Eu, 99.0%) dissolved in concentrated nitric acid (HNO_3, 65%). In addition, commercially available ZnO nanopowder with a particle size of <100 nm was used. All chemicals were purchased from Sigma-Aldrich and used without further purification.

2.2. Characterization Techniques

The morphology and size distribution of the ZnO NPs were examined using atomic force microscopy (AFM, NT-MDT) and optical microscopy (OM, Zeiss). The crystal structure of both pristine and Eu-doped ZnO NPs was analyzed by X-ray diffraction (XRD) using a Rigaku MiniFlex diffractometer with Cu-Kα radiation (λ = 1.5406 Å). XRD patterns were recorded in the 2θ range of 20°–80° with a scanning rate of 2°/min. UV–Vis absorption spectra were obtained using a Specord 250 Plus spectrophotometer. Photoluminescence (PL) properties were investigated using a Cary Eclipse Varian fluorescence spectrophotometer.

2.3. Synthesis of Samples

2.3.1. Synthesis of ZnO Nanoparticles

ZnO NPs were synthesized via a chemical co-precipitation method. A 0.25 M aqueous solution of $Zn(CH_3COO)_2 \cdot 2H_2O$ was used as the zinc precursor, while a 0.625 M NaOH solution served as the precipitating agent. The zinc acetate solution was stirred magnetically for 20 minutes. Subsequently, the NaOH solution was added dropwise under continuous stirring at room temperature, and the reaction was maintained for 4 hours, resulting in the formation of a white precipitate. The product was washed several times with ethanol and distilled water using centrifugation to remove residual ions and byproducts. Finally, the precipitate was dried in a vacuum oven at 60 °C for 4 hours [16]. The sample obtained via this route was

designated as ZnO(S).

2.3.2. Synthesis of $Eu(NO_3)_3 \cdot xH_2O$ as Dopant Source

To facilitate doping, europium nitrate hydrate ($Eu(NO_3)_3 \cdot xH_2O$) was used due to its superior solubility and more effective incorporation of Eu^{3+} ions into ZnO. It was prepared by reacting europium metal with concentrated nitric acid under ambient conditions. The solution was evaporated at 50 °C to obtain $Eu(NO_3)_3 \cdot xH_2O$ as a white hygroscopic solid.

2.3.3. Doping of ZnO NPs with Eu^{3+} Ions

Two wet impregnation doping approaches were employed:

- Eu:ZnO(S): Synthesized ZnO(S) nanoparticles doped with Eu^{3+}.
- Eu:ZnO(C): Commercial ZnO(C) nanoparticles doped with Eu^{3+}.

For each sample, 5 g of ZnO was dispersed in 50 mL ethanol + 20 mL distilled water under ultrasonication. A 3 mol% Eu^{3+} solution was prepared by dissolving $Eu(NO_3)_3 \cdot 6H_2O$ in 20 mL distilled water and then added dropwise to the ZnO suspension. The mixtures were stirred for 4 h and dried at 100 °C for 3 h. The designation of all samples is presented in Table 1.

Table 1. Overview of ZnO nanoparticle samples and the europium doping method.

Sample	Description
ZnO(S)	ZnO synthesized by co-precipitation
ZnO(C)	Commercial ZnO nanopowder
Eu:ZnO(S)	ZnO(S) doped with Eu^{3+} (wet impregnation)
Eu:ZnO(C)	ZnO(C) doped with Eu^{3+} (wet impregnation)

3. Results and Discussion

3.1. Particle Size Distribution Analysis

Figure 1 shows the optical microscopy images of ZnO(C) and ZnO(S) nanoparticles.

AFM images of ZnO NPs: a) ZnO(C) and b) ZnO(S). The ZnO(C) NPs exhibit predominantly spherical morphology with a smooth and uniform surface texture. Their grains appear densely packed, suggesting a relatively narrow size distribution. The lateral grain size of ZnO(C) is estimated to fall in the range of ∼50–100 nm. By contrast, the ZnO(S) NPs synthesized via the co-precipitation method display grains with more pronounced boundaries and a wider size distribution, typically ranging from ∼60–100 nm or larger.

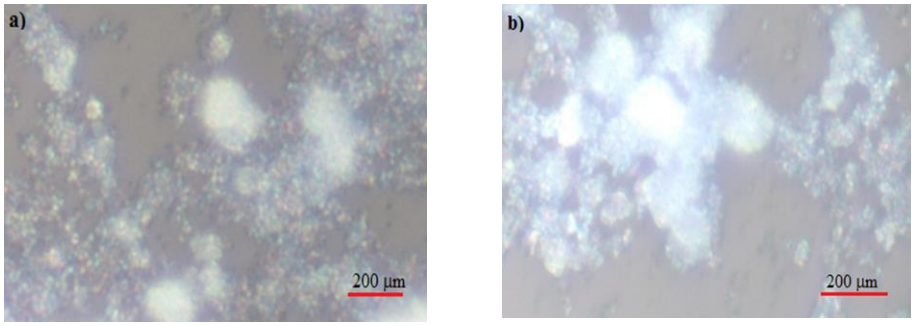

Figure 1. Optical microscopy images of ZnO NPs: a) ZnO(C), b) ZnO(S).

AFM images of the same samples are presented in Figure 2.

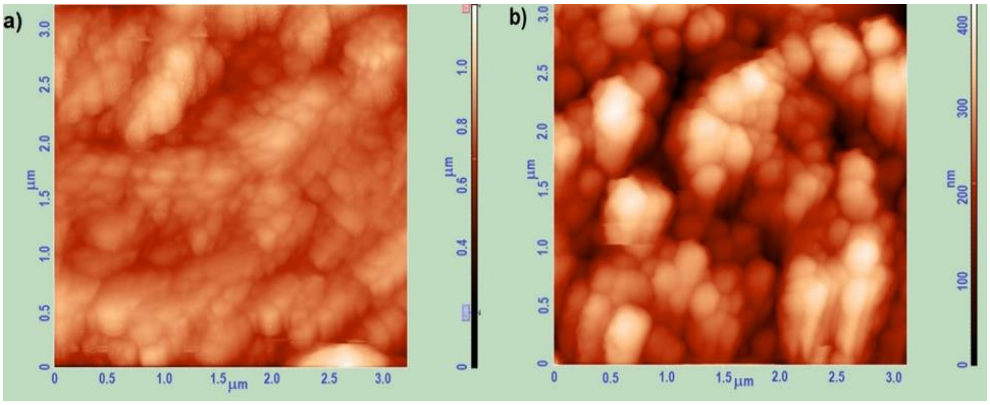

Figure 2. AFM images of ZnO NPs: a) ZnO(C), b) ZnO(S).

The slightly larger grain size and rougher surface observed in ZnO(S) can be attributed to crystal growth processes inherent to the co-precipitation route, which often promotes grain coarsening and partial agglomeration. These morphological differences are expected to influence subsequent doping efficiency, optical responses, and functional performance of the ZnO NPs.

Figure 3 presents the particle size distribution histograms. The particle size distribution of ZnO(C) is mainly concentrated in the 40–80 nm range, with the highest frequency in the 50–70 nm interval. A tail extending toward ~140 nm indicates the presence of a fraction of larger particles, resulting in a somewhat broader distribution. In comparison, ZnO(S) exhibits a more symmetrical distribution, with the peak centered near ~50 nm.

Although both ZnO(C) and ZnO(S) samples show comparable average particle sizes, ZnO(C) demonstrates a wider distribution profile. This variation in size uni-

formity may affect key parameters such as surface area, chemical reactivity, and optical performance, which are critical factors for their application in luminescent and optoelectronic devices.

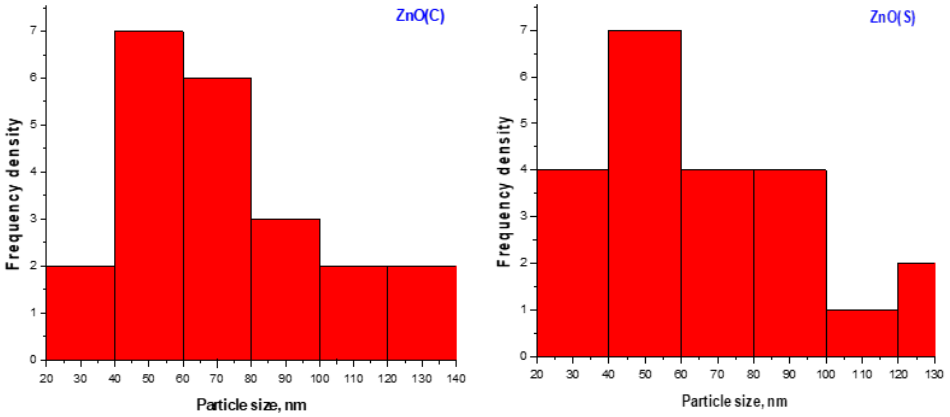

Figure 3. Particle size distribution histograms of ZnO(C) and ZnO(S).

3.2. Crystal Structure of Undoped and Eu^{3+}-Doped ZnO NPs

The crystal structures of the undoped and Eu^{3+}-doped ZnO NPs were analyzed using X-ray diffraction (XRD). Figure 4 shows the XRD patterns of all samples.

The diffraction peaks observed for all samples correspond to the hexagonal wurtzite phase of ZnO, consistent with the standard reference pattern (ICDD PDF 01-070-8072). The lattice parameters are a = 3.2465 Å, b = 3.2465 Å, c = 5.2030 Å, with angles α = β = 90°, γ = 120° [17]. The prominent peak near 36° corresponds to the (101) crystal plane. Table 2 summarizes the main XRD parameter variations of ZnO nanostructures induced by Eu^{3+} doping.

Table 2. Principal XRD characteristics of Eu-doped ZnO nanostructures.

Sample	2θ (°) – Eu:ZnO	2θ (°) – ZnO Reference	Intensity (a.u.) – Eu:ZnO	Intensity (a.u.) – ZnO Reference
Eu:ZnO(S)	35.93	36.23	559.64	2042
Eu:ZnO(C)	36.26	36.45	2000	2222

A clear shift in the 2θ position of the (101) diffraction peak was observed for both ZnO nanoparticle types upon Eu^{3+} doping: from 36.45° to 36.26° in Eu:ZnO(C) and from 36.23° to 35.93° in Eu:ZnO(S). According to Bragg's Law, these shifts toward lower 2θ values indicate an increase in interplanar spacing (d-spacing), reflecting

lattice expansion caused by the substitution of smaller Zn^{2+} ions (ionic radius ~0.74 Å) with larger Eu^{3+} ions (~0.95 Å). This incorporation introduces strain into the ZnO lattice, confirming successful doping.

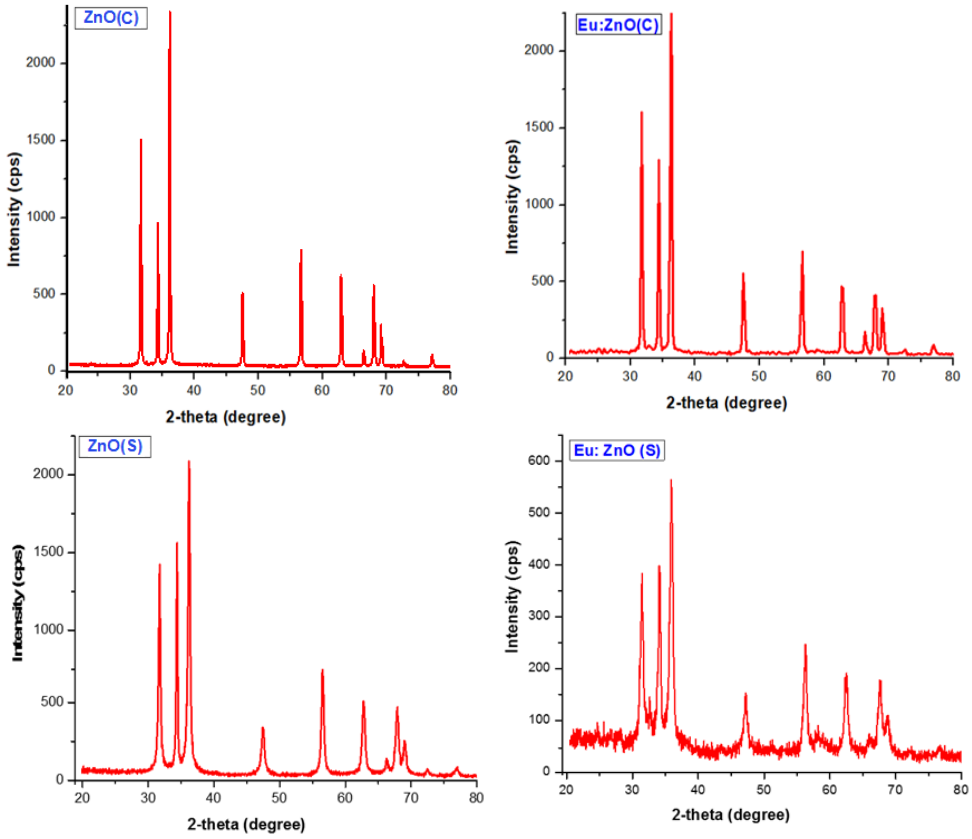

Figure 4. XRD patterns of undoped and Eu^{3+}-doped ZnO NPs.

All Eu-doped samples exhibited reduced diffraction intensities compared to their undoped counterparts, indicating decreased crystallinity likely due to lattice distortion and defect formation. Among the two, Eu:ZnO(S) showed the greatest intensity reduction and lattice distortion, suggesting a stronger structural impact from doping, whereas Eu:ZnO(C) experienced relatively minor changes in crystallinity.

Crystallite sizes, calculated using the Debye–Scherrer equation based on FWHM values of the dominant peaks, were as follows: ZnO(S) – 24 nm, ZnO(C) – 61 nm, Eu:ZnO(S) – 16.01 nm, and Eu:ZnO(C) – 36.06 nm. Eu^{3+} doping led to a reduction in crystallite size for ZnO types. While the absolute decrease was more pronounced in ZnO(C) due to its initially larger size, the smallest crystallites overall were obtained for Eu:ZnO(S), consistent with the greater lattice distortion and defect generation

observed in this sample.

Overall, these results indicate that Eu^{3+} doping affects both the structural integrity and crystallite size of ZnO nanoparticles, with the degree of impact dependent on the nanoparticle source.

3.3. Absorption Properties and Band Gap Analysis of Doped and Undoped ZnO NPs

Figure 5 shows the UV–Vis absorption spectra of undoped ZnO(C) and ZnO(S) nanoparticles.

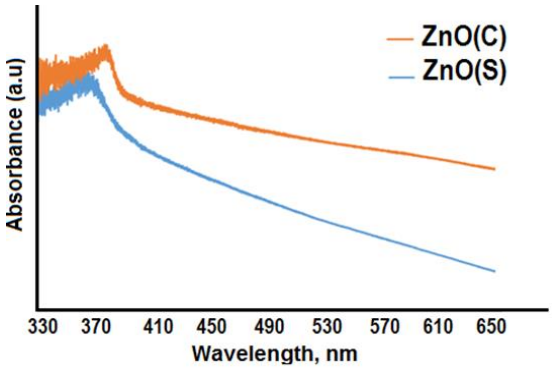

Figure 5. Absorption spectra of ZnO(C) and ZnO(S) NPs.

The ZnO(C) and ZnO(S) samples exhibit distinct optical behaviors. The absorption edge of ZnO(C) appears near ~380 nm, whereas ZnO(S) displays a slight blue shift to approximately ~370 nm. These edges correspond to electronic transitions from the valence band to the conduction band. The shift in ZnO(S) suggests a minor increase in its band gap energy, likely caused by smaller crystallite size or a higher density of intrinsic defects resulting from the co-precipitation synthesis. ZnO(C) also shows increased absorption in the visible region, indicating superior light-harvesting capacity. These findings underscore the influence of synthesis method on the optical absorption characteristics and band structure of ZnO NPs.

The absorption behavior of doped ZnO samples was further investigated. Figure 6 compares the UV–Vis spectra of Eu^{3+}-doped ZnO NPs with their undoped counterparts.

All Eu^{3+}-doped ZnO samples exhibit a primary absorption edge characteristic of the ZnO band-to-band transition. However, a consistent decrease in absorption intensity is observed in the doped samples. This reduction is attributed to the incorporation of Eu^{3+} ions into the ZnO lattice, which leads to the formation of structural defects such as oxygen vacancies and zinc interstitials. These defects introduce localized energy states within the band gap that serve as trap centers for photogenerated charge carriers. As a result, fewer direct transitions between the valence and

conduction bands occur, thus reducing overall absorption intensity.

Additionally, the substitution of divalent Zn^{2+} ions (valence +2) with trivalent Eu^{3+} ions (valence +3) require internal charge compensation, often resulting in the creation of further defects. These defects may promote non-radiative recombination pathways, contributing to the overall decrease in optical absorption intensity [18].

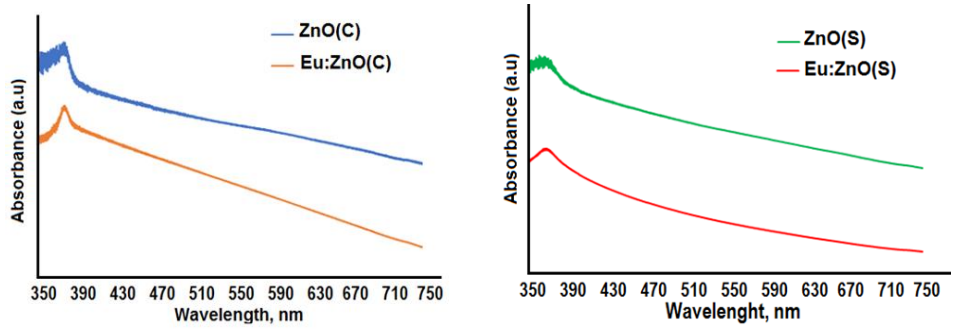

Figure 6. Comparative absorption spectra of doped and undoped ZnO NPs.

All doped samples exhibit a red shift in their absorption edge compared to undoped samples. For example, ZnO(S) shows an absorption edge at ~375 nm, while Eu:ZnO(C) shifts further to the ~390 nm range. This red shift indicates a narrowing of the optical band gap due to Eu^{3+} incorporation.

The band gap narrowing can be explained by the substitution of smaller Zn^{2+} ions (0.74 Å) with larger Eu^{3+} ions (0.95 Å), which introduces lattice distortion and localized states within the band structure. Additionally, defect formation and potential changes in surface morphology contribute to the shift in optical transitions.

In addition, Tauc plots were constructed from the UV–Vis absorption data to estimate the band gap energies, assuming direct allowed transitions (Figure 6). The derived band gap values are summarized in Table 3.

Table 3. Optical band gap (E_g) values of doped and undoped ZnO NPs.

Sample nomination	Doping approach	Optical band gap values
ZnO(C)	Undoped	3.05 eV
ZnO(S)	Undoped	3.00 eV
Eu:ZnO(C)	Wet impregnation	2.95 eV
Eu:ZnO(S)	Wet impregnation	2.9 eV

As shown, Eu^{3+} doping leads to a decrease in the optical band gap for both ZnO(C)

and ZnO(S). These findings support the conclusion that Eu^{3+} doping extends the optical absorption of ZnO into the visible range. Such a shift is highly desirable for applications in optoelectronic and photonic devices that require efficient visible-light response and tunable electronic properties.

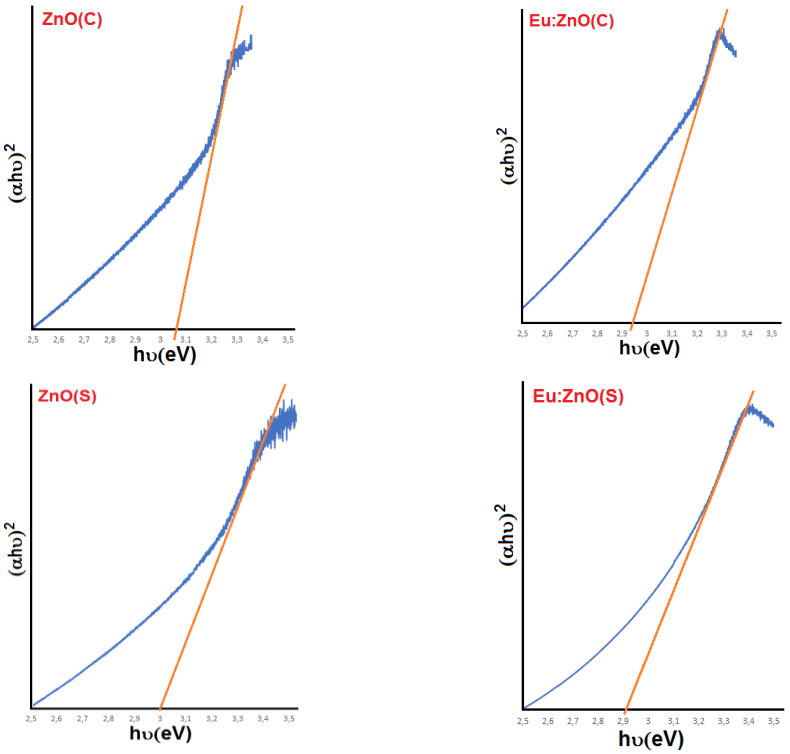

Figure 6. Band gap determination of doped and undoped ZnO NPs using the Tauc plot method.

3.4. Photoluminescence (PL) Properties of ZnO and Eu:ZnO Nanoparticles

Figure 7 presents the comparative PL spectra of undoped ZnO NPs and Eu^{3+}-doped ZnO NPs synthesized by different methods. The PL spectra were recorded with an excitation wavelength of 325 nm. The spectra reveal two main emission regions characteristic of ZnO: a UV emission band below 400 nm and a broad visible emission between 400–700 nm. Distinct emission peaks are observed at ~390 nm, 420 nm, 445 nm, 486 nm, and 501 nm.

The emission at 390 nm corresponds to near-band-edge (NBE) emission of ZnO, attributed to the radiative recombination of free excitons across the intrinsic bandgap (~3.2–3.3 eV). The 420 nm peak is linked to interstitial zinc defects (Zn_i^+), while the 445 nm emission arises from surface-related defects, particularly singly

ionized oxygen vacancies (V_o^+). The 501 nm peak is attributed to interstitial oxygen (O_i) defects, reflecting recombination processes involving deep-level defects [5].

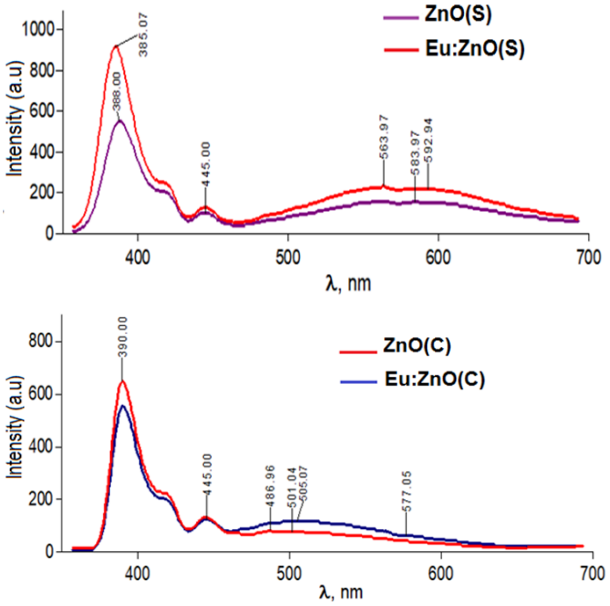

Figure 7. PL spectra of undoped and Eu^{3+}-doped ZnO nanoparticles.

Comparing the spectra of ZnO(C) and Eu:ZnO(C) reveals that doping with Eu^{3+} enhances the emission intensity in the visible region and causes a slight red shift in the emission peak (~505 nm). This enhancement is primarily attributed to the formation of additional structural defects, especially oxygen vacancies, created during Eu^{3+} ion substitution for Zn^{2+} ions. This substitution induces a charge imbalance in the ZnO lattice, which is compensated by defect formation, such as V_o^+ and interstitials. These defects act as radiative recombination centers, thus increasing visible emission [19].

A similar trend is observed when comparing ZnO(S) and Eu:ZnO(S), both synthesized via the wet impregnation method. Emission peaks are detected at ~385 nm, 388 nm, 445 nm, 563 nm, 583 nm, and 592 nm. The broad bands at 563 nm and 583 nm are characteristic of deep-level emission and are generally attributed to a combination of oxygen and zinc vacancies in ZnO nanostructures [20].

Doping ZnO(S) with Eu^{3+} clearly enhances luminescence intensity in both the UV and visible regions. This increase is attributed to the same mechanism discussed above–defect formation due to Eu^{3+} incorporation. These defects introduce deep energy levels within the bandgap that enable radiative recombination of lower-energy photons, thereby shifting the emission spectrum toward the red region.

Notably, a strong emission peak appears at ~592 nm, corresponding to the ^5D_o

$\rightarrow {}^7F_1$ transition of Eu^{3+}. This red emission is a signature of intra-4f transitions in Eu^{3+} ions and confirms the presence of stable luminescent centers embedded in the ZnO matrix.

Among all the doped samples, Eu:ZnO(S) exhibits the most pronounced optical performance. It shows the highest overall PL intensity and a dominant emission peak at 592 nm, confirming effective energy transfer to Eu^{3+} centers and the formation of efficient luminescence pathways. The enhanced yellow-red emission (∼560–590 nm range) makes this sample especially promising for photonics and optoelectronic applications, including red phosphors and visible-light emitters.

4. Conclusion

The effects of europium (Eu^{3+}) doping on the structural, optical, and luminescent properties of ZnO nanoparticles (NPs) were systematically investigated using two different approaches: after synthesis (Eu:ZnO(S)) and using commercial ZnO NPs (Eu:ZnO(C)). Regardless of the doping method, the hexagonal wurtzite structure of ZnO was preserved in all samples.

AFM analysis revealed that ZnO(S) exhibited a more uniform particle size distribution compared to ZnO(C). XRD results showed crystallite sizes of ∼24 nm for ZnO(S) and 61 nm for ZnO(C), with a consistent decrease in crystallite size upon Eu^{3+} doping. The most significant structural alteration was observed in Eu:ZnO(S), where the crystallite size reduced from 24 nm to 16.01 nm, indicating increased lattice strain and reduced crystallinity.

UV–Vis absorption spectra showed absorption edges at 370 nm and 380 nm, correlating with particle size variations. A blue shift (370 nm) in ZnO(S) suggested smaller particles, while a red shift in doped samples (up to ∼390–400 nm) indicated lattice distortion and band gap narrowing. Doping-induced defect states–particularly oxygen vacancies and charge-compensating defects from Eu^{3+} substitution for Zn^{2+}–led to an overall decrease in absorption intensity.

Photoluminescence spectra revealed characteristic emission peaks at 390, 445, 505, and 563 nm, associated with near-band-edge excitonic recombination and intrinsic defect levels. Eu^{3+} doping, whether performed post-synthetically, enhanced visible emission intensity and caused a redshift in emission maxima. This luminescence enhancement is attributed to increased defect density, especially oxygen vacancies, which facilitate efficient radiative recombination.

A distinct emission peak at ∼592 nm, corresponding to the ${}^5D_o \rightarrow {}^7F_1$ transition of Eu^{3+}, confirmed the successful incorporation of Eu^{3+} luminescent centers. These intra-4f transitions, combined with band structure modifications and mid-gap states, enabled sub-band-gap optical transitions and visible photoluminescence enhancement.

The combined UV–Vis and XRD analyses demonstrate a direct correlation bet-

ween Eu^{3+}-induced lattice distortions and the optical behavior of ZnO NPs. Structural changes such as lattice expansion, crystallinity reduction, and defect formation explain the observed redshifts in absorption and emission, as well as the narrowing of the band gap–particularly notable in Eu:ZnO(S).

In conclusion, Eu:ZnO(S) exhibits the most pronounced structural and optical modifications, making it the most promising candidate for applications requiring enhanced luminescence efficiency, such as in optoelectronic, display, or sensor technologies.

References

[1] Shan, W., Walukiewicz, W., Ager, J. W., Yu, K. M., Yuan, H. B., Xin, H. P., Cantwell, G., & Song, J. J. (2005). Nature of room-temperature photoluminescence in ZnO. *Applied Physics Letters, 86*(19), 191911. https://doi.org/10.1063/1.1923757

[2] Willander, M., Nur, O., Sadaf, J. R., Qadir, M. I., Zaman, S., Zainelabdin, A., Bano, N., & Hussain, I. (2010). Luminescence from zinc oxide nanostructures and polymers and their hybrid devices. *Materials, 3*(4), 2643–2667. https://doi.org/10.3390/ma3042643

[3] Shweta, N., Pal, K., & Thapa, K. B. (2019). Synthesis and characterization of ZnO nanoparticles for solar cell application by the cost-effective co-precipitation method without any surfactants. *AIP Conference Proceedings, 2142*(1), 030008. https://doi.org/10.1063/1.5122336

[4] Hanna, B., Manuraj, M., Surendran, K. P., & Unni, K. N. N. (2020). Opto-electronic properties of solution-processed zinc oxide thin films: Role of solvents and doping. *Journal of Materials Science: Materials in Electronics, 31*(19), 13570–13577.

https://doi.org/10.1007/s10854-020-03913-7

[5] Lin, J., Patil, R. A., Devan, R. S., Liu, Z., Wang, Y., Ho, C., Liou, Y., & Ma, Y. (2014). Photoluminescence mechanisms of metallic Zn nanospheres, semiconducting ZnO nanoballoons and metal–semiconductor Zn/ZnO nanospheres. *Scientific Reports, 4*, 6967. https://doi.org/10.1038/srep06967

[6] Raha, S., & Ahmaruzzaman, M. (2022). ZnO nanostructured materials and their potential applications: Progress, challenges and perspectives. *Nanoscale Advances, 4*(7), 1868–1925. https://doi.org/10.1039/d1na00880c

[7] Carofiglio, M., Barui, S., Cauda, V., & Laurenti, M. (2020). Doped zinc oxide nanoparticles: Synthesis, characterization and potential use in nanomedicine. *Applied Sciences, 10*(15), 5194. https://doi.org/10.3390/app10155194

[8] Ishizumi, A., Taguchi, Y., Yamamoto, A., & Kanemitsu, Y. (2005). Luminescence properties of ZnO and Eu^{3+}-doped ZnO nanorods. *Thin Solid Films, 486*(1–2), 50–52. https://doi.org/10.1016/j.tsf.2004.11.229

[9] Lima, S., Sigoli, F., Jafelicci, M., Jr., & Davolos, D. (2001). Luminescent properties and lattice defects correlation on zinc oxide. *International Journal of Inorganic Materials, 3*(7), 749–754. https://doi.org/10.1016/S1466-6049(01)00055-1

[10] Kumar, R., & Dosanjh, H. S. (2022). A mini review on rare earth metal doped ZnO nanomaterials for photocatalytic remediation of wastewater. *Journal of Physics: Conference Series, 2267*(1), 012139. https://doi.org/10.1088/1742-6596/2267/1/012139

[11] Yang, X., Tang, B., & Cao, X. (2023). The roles of dopant concentration and defect states in the optical properties of $Sr_2MgSi_2O_7:Eu^{2+}$, Dy^{3+}. *Journal of Alloys and Compounds, 949*, 169841. https://doi.org/10.1016/j.jallcom.2023.169841

[12] Patra, A., Friend, C. S., Kapoor, R., & Prasad, P. N. (2003). Fluorescence upconversion properties of Er^{3+}-doped TiO_2 and $BaTiO_3$ nanocrystallites. *Chemistry of Materials, 15*(18), 3650–3655. https://doi.org/10.1021/cm020897u

[13] Toma, M., Selyshchev, O., Havryliuk, Y., Pop, A., & Zahn, D. R. T. (2022). Optical and structural characteristics of rare earth doped ZnO nanocrystals prepared in colloidal solution. *Photochem, 2*(3), 515–527. https://doi.org/10.3390/photochem2030036

[14] Mohanty, P., Kim, B., & Park, J. (2007). Synthesis of single crystalline europium doped ZnO nanowires. *Materials Science and Engineering: B, 138*(3), 224–227. https://doi.org/10.1016/j.mseb.2007.01.007

[15] Barsisa, G., Belay, A., Beyene, G., Seboka, C., & Gudishe, K. (2022). Synthesis of europium (Eu^{3+}) doped zinc oxide nanoparticles via the co-precipitation method for photocatalytic applications. *Nano Biomedicine and Engineering, 14*(1), 58–70. https://doi.org/10.5101/nbe.v14i1.p58-70

[16] Kannan, J. A., & Balasubramanian, K. (2020). Thermally influenced optical and fluorescence properties of zinc oxide nanoparticles for glutathione sensing. *Applied Physics A, 126*(7), 598. https://doi.org/10.1007/s00339-020-03780-3

[17] Ghosh, A., Kumari, N., Choudhury, S. P., Tewari, S., & Bhattacharjee, A. (2022). Enhanced blue-shift of the optical band gap in Cd-doped ZnO nanoparticles. *Materials Today: Proceedings, 68*, 215–222. https://doi.org/10.1016/j.matpr.2022.08.164

[18] Ntwaeaborwa, O. M., Mofokeng, S. J., Kumar, V., & Kroon, R. E. (2017). Structural, optical and photoluminescence properties of Eu^{3+} doped ZnO nanoparticles. *Spectrochimica Acta Part A: Molecular and Biomolecular Spectroscopy, 182*, 42–49. https://doi.org/10.1016/j.saa.2017.03.067

[19] Van Dijken, A., Meulenkamp, E., Vanmaekelbergh, D., & Meijerink, A. (2000). The luminescence of nanocrystalline ZnO particles: The mechanism of the ultraviolet and visible emission. *Journal of Luminescence, 87–89*, 454–456. https://doi.org/10.1016/S0022-2313(99)00482-2

[20] Ghrib, T., Al-Otaibi, A. L., Massoudi, I., Alsagry, A. M., Aljaber, A. S., Alhussain, E. A., Alrubian, W. S., Brini, S., Gondal, M. A., Elsayed, K. A., & Kayed, T. S. (2022). Effect of europium doping on the microstructural, optical, and photocatalytic properties of ZnO nanopowders. *Arab Journal of Basic and Applied Sciences, 29*(1), 138–149. https://doi.org/10.1080/25765299.2022.2071525